Ecological Indicators 97 (2019) 150–158

Contents lists available at ScienceDirect

Ecological Indicators

journal homepage: www.elsevier.com/locate/ecolind

Assessing the spatial-temporal pattern and evolution of areas sensitive to land desertification in North China

Duanyang Xu[a,*], Xiaogang You[b], Chunlin Xia[b,*]

[a] Institute of Geographic Sciences and Natural Resources Research, Chinese Academy of Sciences, Beijing 100101, China
[b] Liaoning Technical University, Fuxin 123000, China

ARTICLE INFO

Keywords:
Land desertification
Sensitivity
Pattern
Evolution
North China

ABSTRACT

Desertification is a global threat to human beings, and effective desertification control requires an interdisciplinary approach to identify the pattern and evolution of sensitive areas. Based on the ESA (Environmental Sensitive Areas) principles and real desertification conditions in North China, the Land Desertification Sensitivity Index (LDSI) was constructed to identify the pattern of areas sensitive to desertification in 1981–2010 as well as their evolution under different climate change scenarios from 2011 to 2030. The results show that regions with low and medium sensitivity to desertification were dominant in North China, which together accounted for 61.93% of the study region. From 1981 to 2010, the average LDSI of North China experienced a decreasing trend, and sensitive areas were mainly distributed in the east of Horqin grassland, Chaidamu basin, the east of Tarim basin, and Zhungeer basin. For the period of 2011–2030, the average LDSI of the whole research region also deceased under both RCP4.5 and RCP8.5 scenarios. However, some regions, e.g., Turpan Hami basin and Zhungeer basin, become more sensitive to desertification. Attention should be paid to desertification control and ecology protection measures in these regions.

1. Introduction

Desertification is a phenomenon of land degradation caused by climate change and human activities in arid and semi-arid regions, which seriously affects and disturbs the survival and sustainable development of human society (UNCCD, 1994). Approximately 6–12 million km^2 of land is suffering desertification, and approximately 1–6% of inhabitants of drylands live in desertified area (World Bank, 2009). In 1990s, the United Nations Convention to Combat Desertification Conference on Desertification focused global attention on combating desertification (UNCCD, 1994). In the 21st century, the Millennium Ecosystem Assessment was launched in 2001 and the 2030 Agenda for Sustainable Development was established by the UN in 2015, and both of these efforts emphasized the importance of linking the ecosystem services provided by deserts and desertified land to human well-being (Millennium Ecosystem Assessment, 2005; UNCCD, 2012; Reed et al., 2015).

Identifying the areas sensitive to land desertification and assessing their spatio-temporal pattern and evolution trend provide an important basis for planning desertification control and ecology protection measures (Sterk et al., 2016). The desertification sensitive areas refer to the locations that exhibit a possibility of desertification due to the presence of various factors. These factors are often associated with terrain conditions, soil and vegetation characteristics, climate, and human drivers (Symeonakis et al., 2016; Karamesouti et al., 2018). The Environmental Sensitivity Area (ESA) method that was originally derived from the Mediterranean Desertification and Land Use Project (MEDALUS) funded by the European Union has been used to assess land degradation or desertification sensitivity by constructing an Environmental Sensitivity Area Index (ESAI) from soil, climate, vegetation, and land management (Kosmas et al., 1999; Salvati and Bajocco, 2011; Salvati and Ferrara, 2015). Due to the benefits of ESA principles, such as simplicity, flexibility, and rapid implementation (Contador et al., 2009; Prăvălie et al., 2017), this method has been applied worldwide to evaluate land degradation and desertification risks (Benabderrahmane and Chenchouni, 2010; Tavares et al., 2015; Symeonakis et al., 2016; Karamesouti et al., 2018). In turn, these applications also provided data that can be used to improve this model (Ladisa et al., 2012). For example, Izzo et al (2013) modified the index in the MEDALUS model and applied it in the Dominican Republic. Jafari and Bakhshandehmehr (2016) fused the index and fuzzy logic to quantify the environmental sensitivity to desertification in central Iran. In order to overcome the limitations of the MEDALUS protocol, Duro et al. (2014) proposed the ESPI index and applied it to sensitive areas in the Sicily region, over

* Corresponding authors.
E-mail addresses: xudy@igsnrr.ac.cn (D. Xu), lngdchxyxcl@163.com (C. Xia).

https://doi.org/10.1016/j.ecolind.2018.10.005
Received 16 July 2018; Received in revised form 20 September 2018; Accepted 3 October 2018
Available online 10 October 2018
1470-160X/ © 2018 Elsevier Ltd. All rights reserved.

eight decades of investigation (1921–2000). Salvati and Ferrara (2015) introduced the FIRISK index as a reliable indicator to assess fire risk within the ESAI framework. Prăvălie et al. (2017) assessed the land degradation sensitive areas in southwestern Romania by adjusting the sub-indicators of MEDALUS method based on the local conditions.

China is one of the many countries that have seriously suffered from land desertification. According to the Fifth National Desertification Survey statistics, the area of desertified land in China reached 1,721,200 km^2 in 2014 (State Forestry Administration of China, 2015). The central and local governments have made efforts to combat desertification through various efforts, including the Grain for Green Project, the Beijing and Tianjin Sandstorm Source Treatment Project, the Natural Forest Protection Project, and the "no grazing" statute (Zhang et al., 2012; Xu et al., 2014; Tan and Li, 2015; Xie et al., 2015). However, rapid urbanization, intensive mining and unreasonably afforestation are adding to pressure on desertified land (Cao, 2008; Ge et al., 2016). These trends in conjunction with climate change have led to great desertification risk in North China (Wang et al., 2017). Although previous studies have been conducted to investigate the areas sensitive to land degradation in China via the ESA method (Wang et al., 2014; Sun and Wang, 2015), the method could not be directly used for identifying the areas sensitive to desertification. This is because the ESA indicators and their reference values were derived from MEDALUS and were designed for studying land degradation in the Mediterranean region. Therefore, the ESA method cannot fully reflect the real desertification conditions in North China. Meanwhile, previous studies have largely ignored the prediction of sensitive area change in the future. The prediction of these areas is crucial to support desertification control planning and policy implementation. Therefore, the aims of this paper are to (1) investigate the spatio-temporal pattern of areas sensitive to land desertification in North China from 1981 to 2010 by modifying the ESA method; and (2) to predict the evolution trend of areas sensitive to desertification in North China from 2011 to 2030. The results of this study will hopefully provide a scientific basis to identify key regions for desertification control in China.

2. Materials and methods

2.1. Study area

The desertified areas in China are mainly distributed in the northern regions across the semi-humid, semi-arid, and arid zone, which span 9 provinces (Inner Mongolia, Xinjiang, Qinghai, Ningxia, Gansu, Hebei, Shanxi, Shaanxi, and Sichuan) as well as 222 counties (Wang et al., 2004). The climate characteristics of this region exhibit significant spatial heterogeneity. The average annual precipitation is only 0–450 mm, and it is unevenly distributed in different seasons and regions. Generally, approximately 70–80% of rainfall is concentrated from June to September. The average temperature is approximately 5.7 °C, the average annual sunshine duration is 2807 h, and the average wind speed reaches 2.3 m/s. Most of soils in this area are chestnut soil, brown soil, brown desert soil, mattic soil, and sandy soil. The land cover in the study area also exhibit a high level of spatial heterogeneity, including oasis irrigation agriculture, rainfed agriculture, semi-humid and semi-arid steppe grassland, desert grassland, and alpine meadow steppe. The environment and ecological background of the study region is fragile; and the rapid increases in the population, urbanization, and intensive mining activities have created pressure on the land and increased sensitivity to land desertification (Xu and Ding, 2018).

To facilitate statistical and comparative analyses, the study area was divided into 20 sub-regions according to the climate characteristics and natural geography (Wang et al., 2004) (Fig. 1). The sub-regions include the following: Hulun Buir grassland (hlbr), Horqin grassland (horq), Hunshandake sandy land (hsdk), Chahar grassland (char), Bashang area (bash), Wumeng Qianshan and Tumote plain (wmt), the northwest area of Shanxi Province (jxb), Erdos grassland (erdos), Ningxia Hedong sandy land (nxhd), Three-River Headwaters region (trhr), Chaidamu basin (cdm), Alashan plateau (alsh), Hetao plain (htpy), Hexi Corridor (hxzl), the Houshan region in Inner Mongolia (nmhs), Tarim basin (talm), Turpan Hami basin (thpd), Yinchuan plain (ycpy), Yili basin (ylpd), and Zhungeer basin (zhgr).

2.2. Data sources and preprocessing

The data used in this study include climate, soil, vegetation, topography, Normalized Difference Vegetation Index (NDVI), and socio-economic statistics. The monthly average meteorological data from 1981 to 2010, including temperature, precipitation, sunshine duration, and average wind speed, recorded by meteorological stations in the research region were obtained from the National Meteorological Information Center. The monthly average temperature and precipitation data under the Representative Concentration Pathways 4.5 (RCP4.5) and RCP8.5 scenarios from 2011 to 2030 were acquired from the Climate Change Prediction Dataset of China V3.0 provided by the National Climate Center, which was simulated by using RegCM4.0 that one-way nesting the BCC_CSM1.1 and the resolution of this dataset was 0.5° × 0.5°. A 1:1,000,000 soil map, a vegetation map, a Digital Elevation Model (DEM), and a land use map with 1 km × 1 km resolution were obtained from the Resource Environmental Data Center, Chinese Academy of Sciences. The 8-km resolution and 15-day maximum value composite NDVI data from 1981 to 2010 were obtained from the GIMMS (Global Inventor Modeling and Mapping Studies) NDVI 3 g dataset, which had been pre-processed by geometric correction and graphics enhancement. The GIMMS is widely used in long-term vegetation and land dynamics monitoring (Tian et al., 2015; Georganos et al., 2017). The social-economic statistics at the county scale, such as population and livestock number, were collected from the Statistic Yearbooks of the related provinces in North China. To facilitate spatial analysis and comparison, all the raster data and vector data used in this study were resampled or converted into raster data with an 8-km resolution, and the coordinate system was set to Clarke_1866_Albers.

2.3. Methods

2.3.1. Identification of areas sensitive to land desertification

Based on the principles and major indicators of ESA and the actual characters of land desertification in North China, a Land Desertification Sensitivity Index (LDSI) was constructed from four aspects: the Climate Quality Index (CQI), the Soil Quality Index (SQI), the Vegetation Quality Index (VQI), and the Land Management Quality Index (LMQI). The indicators of LDSI are listed in Table 1.

2.3.1.1. Climate quality index. The Climate Quality Index reflects the impact of climate variation on land desertification, and it was modeled via rainfall, slope aspect, an aridity/humidity index, and a wind erosion index (Table 2). Rainfall is the most important factor for vegetation growth and desertification evolution in arid and semi-arid regions (Hickler et al., 2005; Georganos et al., 2017). Slope aspect determines the distribution of solar irradiation and land surface temperatures, which have significant effects on vegetation growth. The aridity/humidity index and the wind erosion index reflect the impacts of the water-heat balance and wind erosion on land desertification, respectively, and smaller values of the aridity/humidity index and the wind erosion index indicate a lower sensitivity to desertification (Wu et al., 2005; Li et al., 2018).

$$Ia = ET0/P \tag{1}$$

$$C = \frac{1}{100}\sum_{i=1}^{12} \bar{u}^3 \left(\frac{ET_{0i} - P_i}{ET_{0i}}\right) d \tag{2}$$

$$ET0 = 0.19(20 + T)^2(1-r) \tag{3}$$

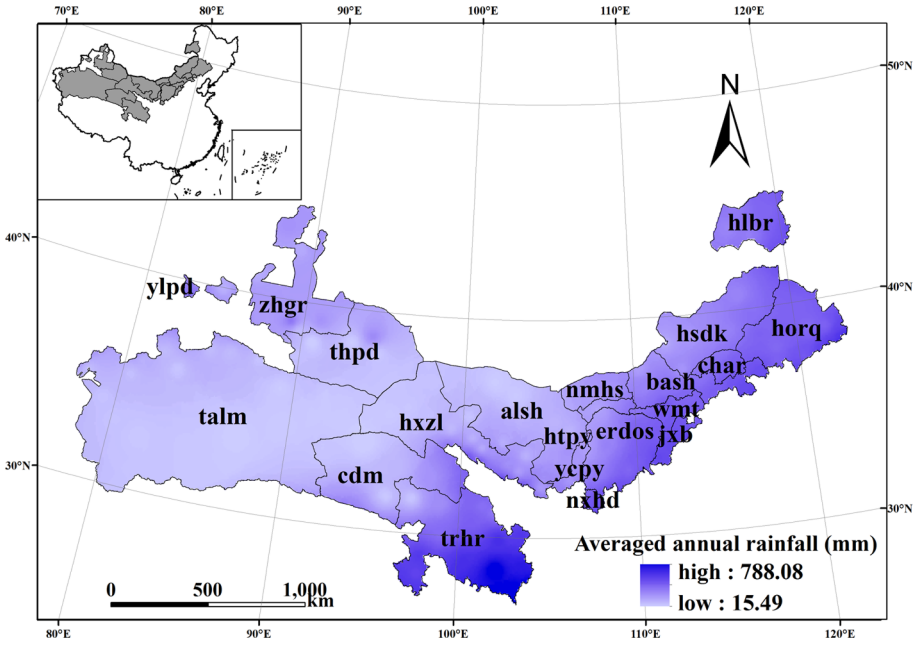

Fig. 1. The location of study area.

where, Ia is the aridity/humidity index (mm/mm); ET_0 is potential evapotranspiration (mm); P is precipitation (mm); C is wind erosion; $\bar{u}$ is average monthly wind at 2 m-height (m/s); d is the days of the month; T is average monthly temperature; and r is monthly mean relative humidity.

2.3.1.2. Soil quality index. The Soil Quality Index measures the influence of terrain conditions and soil parent material on land desertification, and it includes slope, soil texture, and soil depth (Table 3). A higher slope results in less soil stability and a higher sensitivity to desertification (Ferrara et al., 2012). Soil texture and depth also have significant impacts on land desertification. Soils with lower depth and higher sand content are characterized by a lower water-holding capacity and higher erodibility (Liu et al., 2007). These features lead to a higher sensitivity to desertification. All of data used to model SQI were derived from the DEM and the soil map.

2.3.1.3. Vegetation quality index. The Vegetation Quality Index reflects the influence of different vegetation coverage and vegetation types on land desertification. The characteristics of vegetation incorporated into this index are vegetation coverage, erosion protection, and drought resistance (Table 4). In this study, vegetation coverage was replaced by NDVI. A higher NDVI indicates a lower sensitivity to land desertification. Different vegetation types have different responses to erosion and drought (Li et al., 2018). Generally, it is believed that shrub and grass species exhibit good erosion protection and drought resistance (Maestre et al., 2009).

Table 2
Factors and weights of Climate Quality Index (CQI).

Classifications	Factors	Sensitive Class	Scope	Weight
Climate Quality	Rainfall	1	> 465	1.00
		2	275–465	1.33
		3	130–275	1.67
		4	< 130	2.00
	Aridity/ humidity Index	1	< 1.00	1.00
		2	1.00–1.50	1.33
		3	1.50–4.00	1.67
		4	> 4.00	2.00
	Wind Erosion Index	1	< 35	1.00
		2	35–90	1.33
		3	90–310	1.67
		4	> 310	2.00
	Slope Aspect	1	Flat	1.00
		2	West, Northwest, North	1.33
		3	Northeast, East	1.67
		4	Southeast, South, Southwest	2.00

Table 1
Variables, units and data sources in LDSI.

Index	Variables	Units	Data Sources
Climate Quality Index (CQI)	Rainfall (RAI)	mm	National meteorological information center
	Aridity/humidity Index (ARI)	mm/mm	National meteorological information center
	Wind Erosion Index (WER)	Sensitive Class	National meteorological information center
	Slope Aspect (ASP)	Sensitive Class	Resource environment data center of Chinese academy of sciences
Soil Quality Index (SQI)	Slope (SLO)	Degree	Resource environment data center of Chinese academy of sciences
	Texture (TEX)	%	Resource environment data center of Chinese academy of sciences
	Soil Depth (SDP)	cm	Resource environment data center of Chinese academy of sciences
Vegetation Quality Index (VQI)	Vegetation Cover (PLA)	–	Global Inventor Modeling and Mapping Studies
	Erosion Protection (EPT)	Sensitive Class	Resource environment data center of Chinese academy of sciences
	Drought Resistance (DRT)	Sensitive Class	Resource environment data center of Chinese academy of sciences
Land Management Quality Index (LMQI)	Grazing Pressure (GRP)	unit/km^2	Statistical yearbook of the northern provinces
	Population Pressure (DEN)	unit/km^2	Statistical yearbook of the northern provinces

Table 3
Factors and weights of Soil Quality Index (SQI).

Classifications	Factors	Sensitive Class	Scope	Weight
Soil Quality	Slope	4	> 3.28	2.00
		3	1.64–3.28	1.67
		2	0.64–1.64	1.33
		1	< 0.64	1.00
	Texture	1	< 25	1.00
		2	25–40	1.33
		3	40–65	1.67
		4	> 65	2.00
	Soil Depth	1	Brown coniferous forest soil, Brown soil, Dark brown forest soil, Cinnamon soil, Gray cinnamonic soil, Black soil, Grey forest soil, Chernozems, Bog soil	1.00
		2	Chestnut soil, Castano-cinnamon soil, Dark loessial soil, Brown soil, Sierozem, Meadow solonchaks, Shruby meadow soil, Fluvo-aquic soil, Grass mat soil, Frigid calcic soil, Cold calcic soil	1.33
		3	• Gray desert soil, Gray-brown desrt soil, Brown desert soil, Loessial soil, Alluvial soil, Takyr, Meadow soils, Solonchak, Desert solonchaks, Frigid plateau solonchaks, Solonetz, Irrigated desert soils, Cold desert soil, Northwest salt crust	1.67
		4	Aeolian sandy soil, chisley soil, skeleton soil	2.00

2.3.1.4. Land management quality index. The Land Management Quality Index reflects the impact of human activities on land desertification (Table 5). In North China, the pressures from grazing and rural population are two of the most important factors that lead to desertification. Both of these factors are selected to model LMQI. Grazing pressure was calculated by the density of livestock, which was expressed in sheep units. Large animals, mainly including cows, horses, and donkeys, were converted to five sheep units (Xin et al., 2011). Rural population pressure was computed by the density of rural people in each county. However, the impact of grazing prohibition policy and urbanization were not considered in this study; so, the LMQI only measures the potential or maximum impact of grazing and rural population.

$$GPRn = \frac{SUn}{Sn} \quad (4)$$

$$DENn = \frac{PEn}{Sn} \quad (5)$$

where, $GPRn$ is the grazing pressure; SU_n is the number of sheep units in county n; S_n is the area that is influenced by grazing and rural population, which refers to the grassland and unutilized land in this study; and PE_n is the number of rural population in county n.

2.3.1.5. LDSI modeling and classification. According to the original methodology of ESA, each LDSI parameter was classified into four classes by using the natural breaks criterion or by referencing its degree of influence on desertification (Jenks, 1977; Prăvălie et al., 2017), and the four classes of parameters were weighted with a score between 1 (low sensitivity to land desertification) and 2 (high sensitivity to land desertification). Based on the weighted geometric mean method, CQI, SOI, VQI, and LMQI were calculated to construct the LDSI. Finally, LDSI was reclassified into four classes by using the natural breaks criterion: non sensitivity (LDSI < 1.273), low sensitivity (1.273 < LDSI < 1.388), medium sensitivity (1.388 < LDSI < 1.490), and high sensitivity (LDSI > 1.490).

Table 5
Factors and weights of Land Management Quality Index (MQI).

Classifications	Factors	Sensitive Class	Scope	Weight
Land Management Quality	Grazing Pressure	1	< 20	1.00
		2	20–105	1.33
		3	105–330	1.67
		4	> 330	2.00
	Population Pressure	1	< 15	1.00
		2	15–45	1.33
		3	45–75	1.67
		4	> 75	2.00

$$SQI_{ij} = (SLO_{ij} \times TEX_{ij} \times SDP_{ij})^{1/3} \quad (6)$$

$$CQIij = (RAIij \times ARIij \times WERij \times ASPij)^{1/4} \quad (7)$$

$$VQIij = (PLAij \times EPTij \times DRTij)^{1/3} \quad (8)$$

$$LMQIij = (GRPij \times DENij)^{1/2} \quad (9)$$

$$LDSIij = (SQIij \times CQIij \times VQIij \times MQIij)^{1/4} \quad (10)$$

2.3.2. Prediction of areas sensitive to land desertification

The prediction of areas sensitive to land desertification was determined by the values of driving factors in 2011–2030. Some LDSI factors would not change on the scale of decades, such as soil characteristics,

Table 4
Factors and weights of Vegetation Quality Index (VQI).

Classifications	Factors	Sensitive Class	Scope	Weight
Vegetation Quality	Vegetation Cover (NDVI)	1	> 0.34	1.00
		2	0.22–0.34	1.33
		3	0.11–0.22	1.67
		4	< 0.11	2.00
	Erosion Protection	1	Swamp, Broad leaved forest, Coniferous forests, Water, Mixed coniferous broad leaved forest, Alpine vegetation	1.00
		2	• Cropland, Grasslands, Meadow, Thick growth of grass	1.33
		3	Shrubland	1.67
		4	Desert, Rock, Unvegetated area	2.00
	Drought Resistance	1	Broad leaved forest, Coniferous, Mixed coniferous broad leaved forest, Water	1.00
		2	Cropland, Swamp, Alpine vegetation, Shrubland	1.33
		3	Grasslands, Meadow, Thick growth of grass	1.67
		4	Desert, Rock, Unvegetated area	2.00

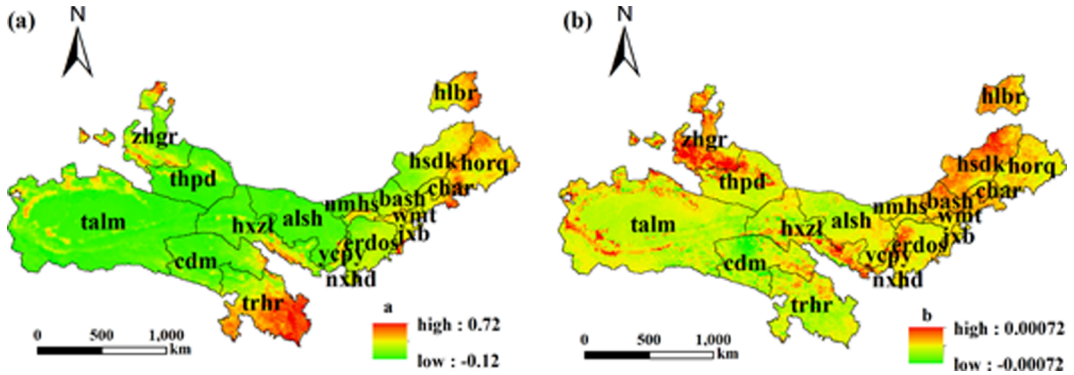

Fig. 2. The spatial distribution of linear regression (a) coefficient and (b) intercept between NDVI and rainfall from 1981 to 2010.

vegetation characters, slope, and slope aspect; and these factors were set to constant values in the model. The monthly average temperature and precipitation data under RCP4.5 and RCP8.5 from 2011 to 2030 were used to model the future values of the aridity/humidity index and the wind erosion index. NDVI from 2011 to 2030 was predicted via a linear regression model according to NDVI and precipitation from 1981 to 2010, which had been proved to be a useful way to estimate the vegetation dynamics in arid and semi-arid region (Fensholt and Rasmussen, 2011; Huber et al., 2011); and the coefficient and intercept at the grid scale are shown in Fig. 2. In terms of land management, the average natural growth rates of population and livestock numbers between 1981 and 2010 were used to simulate the change in rural population, livestock number, and LMQI from 2011 to 2030.

3. Results

3.1. The spatial pattern of areas sensitive to land desertification in North China

According to the spatial distribution of LDSI and its four component indices, the values of these indices were lower in the eastern and southern portion of North China than the western portion (e.g., the average LDSI in hlbr reached 1.25, more lower than 1.44 of talm); and this pattern was basically consistent with rainfall and vegetation, which showed higher value in eastern and southern than western China. The areas with low and medium desertification sensitivities occupied 61.92% of the whole study region, and their total areas reached 8.52×10^5 km^2 and 1.00×10^6 km^2, respectively (Fig. 3). The areas with low desertification sensitivity were mainly located in the eastern part of hsdk, western part of hlbr, horq, and bash. The areas with high desertification sensitivity accounted for 20.92% of the whole study region, and these areas were mainly distributed in the central part of talm, the central part of cdm, and alsh. At the scale of sub-regions, the LDSI of alsh was the highest, with a value of 1.47. The LDSI values of ycpy, talm, thpd, and htpy ranged between 1.40 and 1.45, and these areas therefore were classified as medium and high desertification sensitivity areas. The LDSI of hlbr and trhr was the lowest among sub-regions, reaching 1.26 and 1.24, respectively. Therefore, these areas belong to non desertification sensitivity category.

3.2. The dynamics of areas sensitive to land desertification in North China from 1981 to 2010

The average LDSI during 1981–1985 and 2006–2010 were used to analyze the dynamics of areas sensitive to land desertification in North China. From 1981 to 2010, the spatial pattern of areas sensitive to land desertification did not change greatly. However, the structure of lands with different desertification sensitivities changed obviously. The area of lands with non and medium desertification sensitivities decreased by 4.86×10^4 km^2 and 6.85×10^4 km^2, respectively; and the area of lands with low and high desertification sensitivities increased by 7.33×10^4 km^2 and 4.40×10^4 km^2, respectively (Fig. 4). Over the past 30 years, the average LDSI of the whole study region experienced a decreasing trend, and the regions with decreasing LDSI were mainly distributed in the eastern area of horq, cdm, the eastern portion of talm, and zhgr. The areas with decreasing LDSI values in the aforementioned sub-regions accounted for 10.32%, 16.82%, 9.01%, and 16.24% of the total study area, respectively. The increasing rainfall and the reductions in the aridity/humidity index and wind erosion index were the main causes of LDSI deceases in these sub-regions. For example, the middle part of cdm exhibited a 29.50% increase in rainfall and the aridity/humidity index and wind erosion index decreased by 23.22% and 59.23%, respectively. These trends benefited the rehabilitation of degraded lands and reduced desertification sensitivity.

The regions with an increasing trend of LDSI were mainly distributed in hsdk, char, the western area of horq, the southeastern portion of hxzl, the west of thpd, and the west of talm. The trends in these areas were mainly attributable to the reduction in rainfall and increase in population pressure. For example, the proportion of lands with non desertification sensitivity in the west of horq greatly decreased in the 1990s. This trend was mainly induced by the increasing population. The rural population pressure of this sub-region increased 67% over the past 30 years. The deceasing rainfall was the key factor that led to the increase of LDSI in hsdk from 1981 to 2010.

3.3. Prediction of areas sensitive to land desertification in North China from 2011 to 2030

The dynamics of LDSI in North China from 2011 to 2030 were predicted via the simulated LMQI and climate-related indices from the RCP4.5 and RCP8.5 scenarios. Under the RCP4.5 scenario, the pattern of lands with different desertification sensitivities would significantly change, and lands with non and low desertification sensitivities would dominate in North China (Fig. 5). Compared with 2010, the areas with non desertification sensitivity would greatly increase in 2030, and this area is almost 2.4 times of that in 2010. The newly predicted increases in areas with non desertification sensitivities are mainly distributed in the western part of hlbr, hsdk, talm, and the southern part of cdm. Decreases in areas with medium desertification sensitivity was another important trend under the RCP4.5 scenario, and the area of lands with medium desertification sensitivity decreased by 19.25% in 2030 (i.e., 5.77e10^5 km^2). Among the regions that moved away from medium desertification sensitivity, 14.58% transferred to high desertification sensitivity. These regions were mainly distributed in the west of thpd, the middle part of zhgr, and talm. These areas should receive more attention due to their higher desertification risk. In the simulation, lands with low desertification sensitivities decreased from 8.98eas^5 km^2 in 2010 to 6.44eas^5 km^2 in 2030.

The pattern of areas sensitive to land desertification in 2030 under the RCP8.5 scenario was similar to the pattern under the RCP4.5

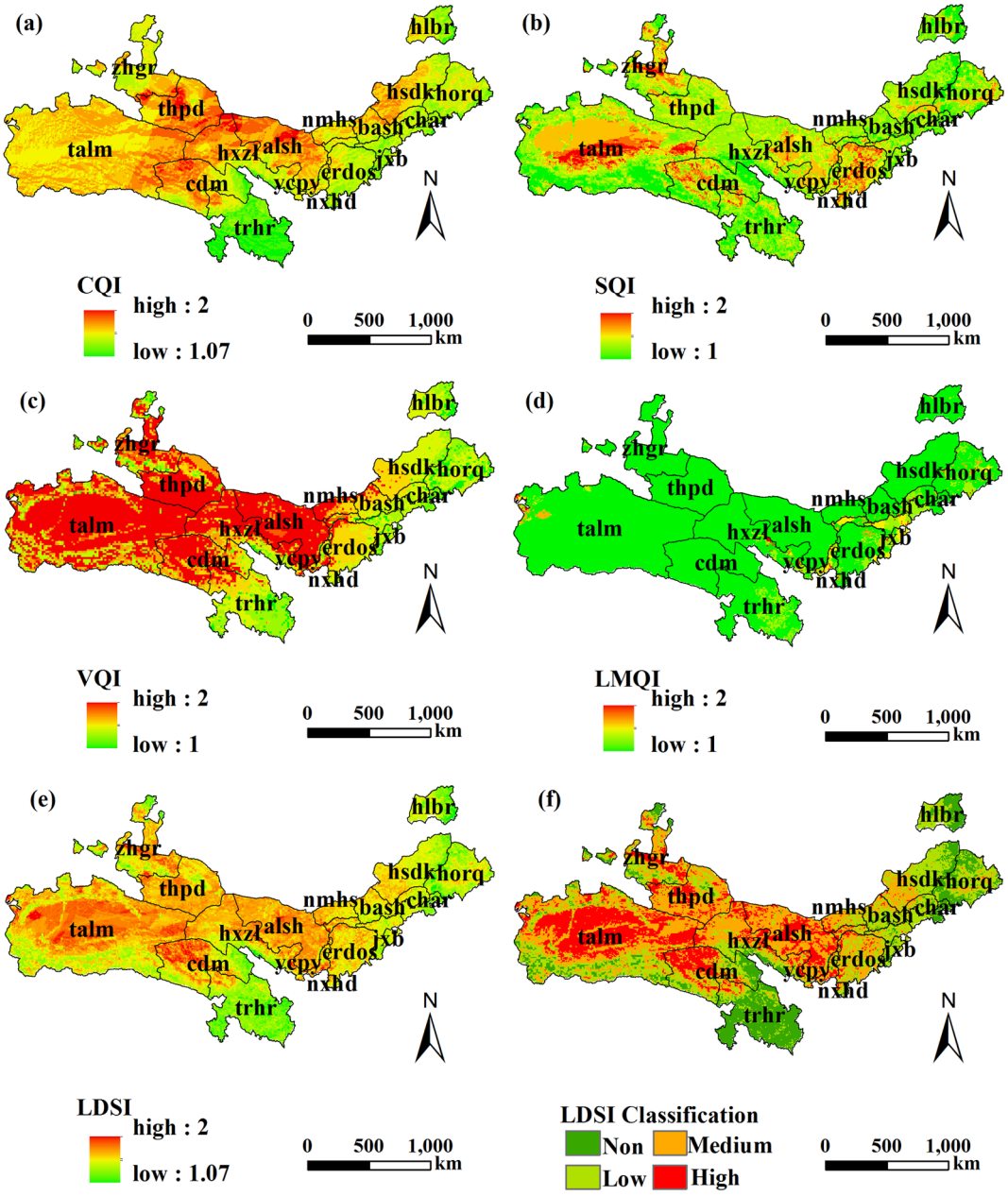

Fig. 3. The spatial pattern of areas sensitive to land desertification in North China (a) Climate Quality Index (CQI); (b) Soil Quality Index (SQI); (c) Vegetation Quality Index (VQI); (d) Land Management Quality Index (LMQI); (e) Land Desertification Sensitivity Index (LDSI); (f) LDSI classification.

scenario. Under the RCP8.5 scenario, the lands with non desertification sensitivity greatly increased. The area of lands with non desertification sensitivity in 2030 reached 1.24 h10^6 km^2, which is approximately 2.77 times the level in 2010. Compared with 2010, areas with low, medium, and high desertification sensitivity in 2030 decreased by 2.45×10^5 km^2, 3.34×10^5 km^2, and 1.17×10^5 km^2, respectively. Although the total area of lands with high desertification sensitivity decreased, the LDSI of some regions rapidly increased and reached the high sensitivity level. These regions were mainly distributed in the west of thpd and the middle part of zhgr. For example, the areas with high sensitivity in thpd and zhgr increased by 37.26% and 15.16%, respectively, from 2011 to 2030.

4. Discussion

Desertification is an important problem in China that impacts the environment and the economy. In previous decades, researchers have paid more attention to desertification dynamics and their relationships to climate change and human activities at local, regional, and national scales (Xu et al., 2014; Zhou et al., 2015; Zhang and Huisingh, 2018). However, the driving forces of desertification have seldom been considered in an integrated framework to and assess the regional sensitivity or to identify areas sensitive to desertification. This research gap could result in a lack of governmental recognition of the regions with higher sensitivities and their predicted future trends. The method and principles of ESA provides a very flexible framework to study and identify the areas sensitive to land desertification in China. By referencing the major indices of ESA (Salvati and Ferrara, 2015; Karamesouti et al., 2018), the LDSI was developed by adjusting the indicator system to fit the reality of desertification in China via the introduction of indicators such as wind erosion, rural population, and pasturage pressure (Wang et al., 2017; Li et al., 2018).

Generally, the pattern of areas sensitive to land desertification in North China exhibited a close relationship with vegetation and rainfall.

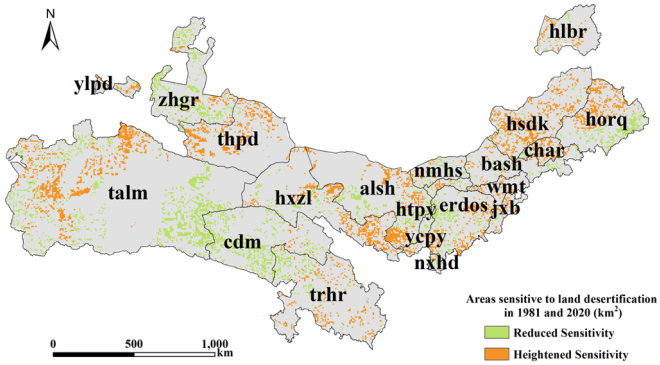

Area(km²)

	Non	Low	Medium	High
1981	594304	824960	994048	583168
2010	545664	898176	925504	627136

Fig. 4. The dynamics of areas sensitive to land desertification between 1981 and 2010.

The lower LDSI values as well as non or low desertification sensitivity areas were mainly distributed in the east of Inner Mongolia and trhr. These areas had a higher vegetation coverage and cumulative annual rainfall that exceeded 300 mm (Shen et al., 2018). In contrast, the higher LDSI values and high sensitivity areas were often located in western China, especially in Xinjiang, Gansu, and Qinghai provinces (e.g., talm, cdm, zhgr, and thpd). This pattern is also consistent with previous studies (Wang et al., 2014). Although human activities did not change the basic spatial pattern of areas sensitive to land desertification in North China, they may have increased the heterogeneity of the pattern at the regional scale. For example, the rapid increase of rural people and livestock in hsdk and horq should increase the land use intensity and LMQI, which would lead to higher LDSI values in these regions (Ge et al., 2016).

However, when the dynamics of areas sensitive to land desertification and LDSI were analyzed from 1981 to 2010, we found that the change in lands with different desertification sensitivities and their driving forces exhibited significant heterogeneity. Over the past 30 years, the rural population and livestock number increased notably in North China (Feng et al., 2015; Xu and Ding, 2018), which would lead an increasing trend of LQMI in the most regions; however, the decreasing LDSI values were investigated in some regions, which had a close relationship with climate change, and they could be attributable to the increasing rainfall and decrease in wind erosion (Wang et al., 2008). For example, Baarin Right Banner in horq experienced an increase in the rural population from 1.21×10^5 in 1981 to 1.26×10^5 in 2010, and the livestock number (expressed in sheep units) also increased by 1.69 times in the past 30 years. However, the aridity index and wind erosion index decreased 3.75% and 36.94% over the same period (Fig. 6). This suggests that climate change in this region benefited desertified land rehabilitation. Meanwhile, ecological engineering projects, such as the Three-North Shelterbelt Project, the Beijing-Tianjin Sandstorm Source Treatment Project, and the Grain for Green Project, would also lead to obvious increases of NDVI (Xu et al., 2014; Tan and Li, 2015). The LDSI increases in hsdk are mainly attributable to the coupled effect of land management pressure and bad climate conditions. Land management played a dominated role, and these regions are mainly located in Sonid Right Banner and Sonid Left Banner. The regions with lower vegetation coverage and rainfall in the western area of North China were more sensitive to desertification given the same human pressures.

Based on analyzing the pattern and evolution of areas sensitive to land desertification in the past, this study attempted to predict the future dynamics of these areas by introducing the simulated climate change data and the related vegetation trends under RCP4.5 and RCP8.5 as well as land management data. With population growth of 7.62% and livestock growth of 3.19%, the simulated average LDSI of the whole research region decreased from 2011 to 2030, which

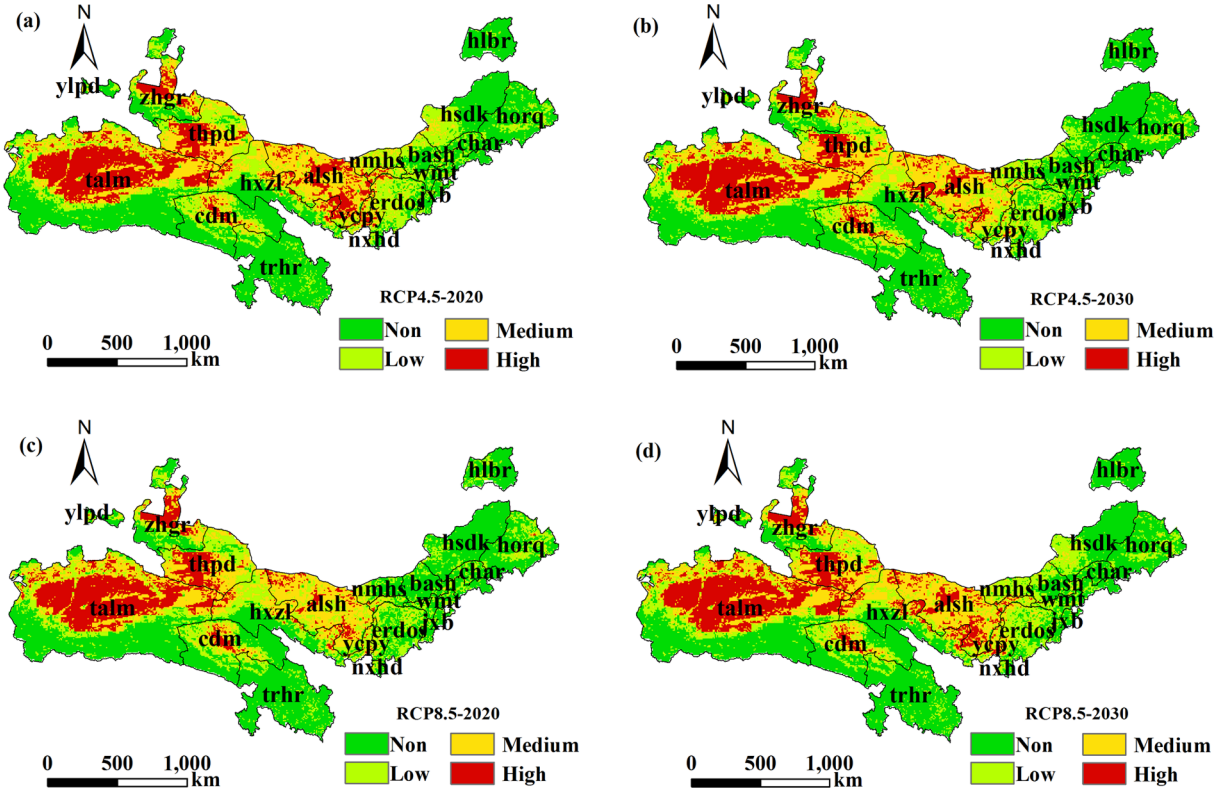

Fig. 5. The spatial distribution of areas sensitive to land desertification in RCP4.5 and RCP8.5 scenarios (a) RCP4.5–2020; (b) RCP4.5–2030; (c) RCP8.5–2020; (d) RCP8.5–2030.

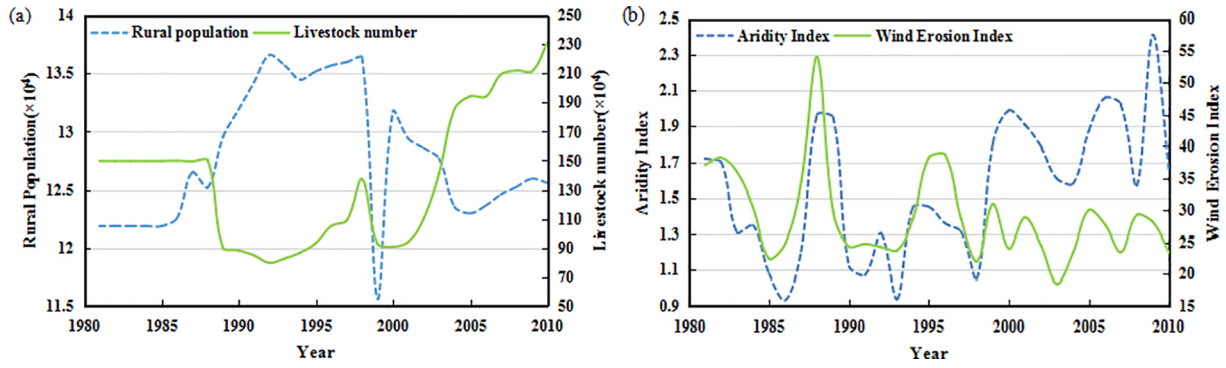

Fig. 6. The change of (a) aridity/humidity index and wind erosion index; (b) rural population and livestock number in Baarin Right Banner from 1981 to 2010.

indicates that areas are tending to transfer from higher levels of sensitivity to lower levels of sensitivity. This trend is mainly attributable to the increasing rainfall in RCP 4.5 and RCP8.5, and this trend has been observed in previous studies (Yu et al., 2014; Hui et al., 2018). However, the rainfall and temperature changes exhibits pronounced heterogeneity. The decreases in rainfall and increases in temperature in some regions would lead to LDSI increases and elevated levels of desertification sensitivity. This pattern is seen in areas such as the western part of thpd and the middle of zhgr. This suggests that these areas have a greater risk of desertification than other sub-regions, and more attention should be paid to desertification control and ecology protection measures in these regions. For example, grazing prohibition policy should be implemented and long-term persisted, water-saving technologies should be widely adopted in the rain-fed farmland, and degraded regions should be repaired by using native drought resistant plants and maintaining it within the ecological carrying capacity (Cao et al., 2009, 2018).

In this study, there were also several sources of uncertainty that were introduced into the modeling of LDSI. First, due to the data accessibility, only population and grazing pressure were considered to assess the impact of land management on desertification. Relevant policy variables, such as ecological engineering projects, grazing prohibitions, urbanization, and population movements were not considered in this study, which might lead to over-estimate the impact of land management on LDSI, because the real number of livestock and rural people that have impact on desertification were always less than the statistic data. In future studies, improvements will be made to the LDSI indicator system. Particular effort will be made to introduce policy variables into the LDSI framework to obtain more accurate information regarding human-induced desertification and rehabilitation processes (Cao et al., 2014). Secondly, the method of vegetation (NDVI) modeling should be improved. Although the model based on the NDVI-rainfall relationship could predict the fundamental trend of NDVI in future, there still exists uncertainties; for example, the lag-effect of rainfall on vegetation and the change of land use would have impact on the accuracy of NDVI-rainfall model at pixel level (Zewdie et al., 2017); so, a process-based model that considers vegetation growth process and land use dynamics should be introduced to simulate vegetation dynamics under different scenarios. Besides, due to the uncertainties of regional climate model, the data of rainfall retrieved from RCP4.5 and RCP8.5 from 2011 to 2030 might also lead uncertainties of model LDSI, which should be compared with other predicted-rainfall dataset to reduce the uncertainties in future study.

5. Conclusions

In this study, the land desertification sensitivity index (LDSI) was constructed by considering climate, soil, vegetation, and land management. The index was used to assess and predict the pattern and evolution of areas sensitive to desertification from 1981 to 2030 in North China. The pattern of areas sensitive to land desertification in North China was basically consistent with the pattern of rainfall and vegetation coverage, and the eastern portion of North China exhibited higher LDSI values than the western portion. Among the lands with different sensitivities to desertification, the areas with low and medium sensitivities occupied 61.93% of the total study area. From 1981 to 2010, the average LDSI of the whole research region experienced a decreasing trend. This is mainly attributed to improvements in the arid/humid environment and reduction of wind erosion, especially in the east of horq, cdm, the east of talm, and zhgr.

For the period of 2011–2030, the simulated pattern of land desertification sensitive areas did not obviously change and the average LDSI of whole research region deceased. This pattern is mainly attributed to the increasing of rainfall and vegetation rehabilitation in arid and semi-arid regions of North China. However, some regions like thpd and zhgr may become more sensitive to desertification, and additional attention should be paid to desertification control and ecological protection in these areas. In future studies, the uncertainty and inaccuracy of LDSI modeling should be mitigated by introducing more social-economic and policy factors.

Acknowledgement

This research is jointly supported by National Program on Key Research Project of China (2017YFC0506704, 2016YFC0501002), and National Natural Science Foundation of China (71573245).

References

Benabderrahmane, M.C., Chenchouni, H., 2010. Assessing environmental sensitivity areas to desertification in eastern Algeria using Mediterranean Desertification and Land Use “MEDALUS” Model. Int. J. Sustain. Water Environ. Syst. 1, 5–10.

Cao, S.X., 2008. Why large-scale afforestation efforts in China have failed to solve the desertification problem. Environ. Sci. Technol. 42 (5), 1826–1831.

Cao, S.X., Liu, Y.J., Yu, Z.Q., 2018. China's successes at combating desertification provide roadmap for other nations. Environ. Sci. Policy. Sustain. Dev. 60, 16–24.

Cao, S.X., Ma, H., Yuan, W.P., Wang, X., 2014. Interaction of ecological and social factors affects vegetation recovery in China. Biol. Conserv. 180, 270–277.

Cao, S.X., Zhong, B.L., Yue, H., Zeng, H.S., Zeng, J.H., 2009. Development and testing of a sustainable environmental restoration policy on eradicating the poverty trap in China's Changting County. PNAS 106 (26), 10712–10716.

Contador, J.F.L., Schnabel, S., Gutierrez, A.G., Fernandez, M.P., 2009. Mapping sensitivity to land degradation in Extremadura. Sw Spain. Land Degrad. Dev. 20, 129–144.

Duro, A., Piccione, V., Ragusa, M.A., Veneziano, V., 2014. New enviromentally sensitive patch index-ESPI-for MEDALUS protocol. In: 10th International Conference on Mathematical Problems In Engineering, 15-18 July 2014, Edited by S. Sivasundaram, Narvik, Norway: Aerospace and Sciences: ICNPAA 2014, AIP Conf. Proc. 1637, pp. 305–318.

Feng, Q., Ma, H., Jiang, X.M., Wang, X., Cao, S.X., 2015. What has caused desertification in China? Sci. Rep.-Uk 5.

Fensholt, R., Rasmussen, K., 2011. Analysis of trends in the Sahelian ‘rain-use efficiency’ using GIMMS NDVI, RFE and GPCP rainfall data. Remote Sens. Environ. 115, 438–451.

Ferrara, A., Salvati, L., Sateriano, A., Nole, A., 2012. Performance evaluation and cost assessment of a key indicator system to monitor desertification vulnerability. Ecol. Indic. 23, 123–129.

Ge, X.D., Dong, K.K., Luloff, A.E., Wang, L.Y., Xiao, J., 2016. Impact of land use intensity on sandy desertification: an evidence from Horqin Sandy Land, China. Ecol. Indic. 61, 346–358.
Georganos, S., Abdi, A.M., Tenenbaum, D.E., Kalogirou, S., 2017. Examining the NDVI-rainfall relationship in the semi-arid Sahel using geographically weighted regression. J. Arid Environ. 146, 64–74.
Hickler, T., Eklundh, L., Seaquist, J.W., Smith, B., Ardo, J., Olsson, L., Sykes, M.T., Sjostrom, M., 2005. Precipitation controls Sahel greening trend. Geophys. Res. Lett. 32, 365–370.
Huber, S., Fensholt, R., Rasmussen, K., 2011. Water availability as the driver of vegetation dynmaics in the African Sahel from 1982 to 2007. Glob. Planet. Change. 76, 186–195.
Hui, P.H., Tang, J.P., Wang, S.Y., Niu, X.R., Zong, P.S., Dong, X.N., 2018. Climate change projections over China using regional climate models forced by two CMIP5 global models. Part II: projections of future climate. Int. J. Climatol. 38, E78–E94.
Izzo, M., Araujo, N., Aucelli, P.P.C., Maratea, A., Sanchez, A., 2013. Land sensitivity to desertification in the dominican republic: an adaptation of the Esa methodology. Land Degrad. Dev. 24, 486–498.
Jafari, R., Bakhshandehmehr, L., 2016. Quantitative mapping and assessment of environmentally sensitive areas to desertification in Central Iran. Land Degrad. Dev. 27, 108–119.
Jenks, G.F., 1977. Optimal Data Classification for Choropleth Maps. University of Kansas, United States.
Karamesouti, M., Panagos, P., Kosmas, C., 2018. Model-based spatio-temporal analysis of land desertification risk in Greece. Catena 167, 266–275.
Kosmas, C., Kirkby, M., Geeson, N., 1999. Manual on Key Indicators of Desertification and Mapping Environmentally Sensitive Areas to Desertification. EUR 18882. European Commission, Energy, Environment and Sustainable Development, Bruxelles.
Ladisa, G., Todorovic, M., Liuzzi, G.T., 2012. A GIS-based approach for desertification risk assessment in Apulia region, SE Italy. Phys. Chem. Earth 49, 103–113.
Li, D.J., Xu, D.Y., Ding, X., Wang, Z.Y., Song, A.L., 2018. Changes of wind erosion climatic erosivity and vegetation dynamics response in northern China from 1981 to 2010. Res. Soil Water Conserv. 25 (2), 15–20 (in Chinese).
Liu, L.Y., Li, X.Y., Shi, P.J., Gao, S.Y., Wang, J.H., Ta, W.Q., Song, Y., Liu, M.X., Wang, Z., Xiao, B.L., 2007. Wind erodibility of major soils in the farming-pastoral ecotone of China. J. Arid Environ. 68, 611–623.
Maestre, F.T., Bowker, M.A., Puche, M.D., Hinojosa, M.B., Martinez, I., Garcia-Palacios, P., Castillo, A.P., Soliveres, S., Luzuriaga, A.L., Sanchez, A.M., Carreira, J.A., Gallardo, A., Escudero, A., 2009. Shrub encroachment can reverse desertification in semi-arid Mediterranean grasslands. Ecol. Lett. 12, 930–941.
Millennium Ecosystem Assessment, 2005. Ecosystems and Human Well-being: Desertification Synthesis. World Resources Institute, Washington, DC.
Pravalie, R., Savulescu, I., Patriche, C., Dumitrascu, M., Bandoc, G., 2017. Spatial assessment of land degradation sensitive areas in southwestern Romania using modified MEDALUS method. Catena 153, 114–130.
Reed, M.S., Stringer, L.C., Dougill, A.J., Perkins, J.S., Atlhopheng, J.R., Mulale, K., Favretto, N., 2015. Reorienting land degradation towards sustainable land management: linking sustainable livelihoods with ecosystem services in rangeland systems. J. Environ. Manage. 151, 472–485.
Salvati, L., Bajocco, S., 2011. Land sensitivity to desertification across Italy Past, present, and future. Appl. Geogr. 31, 223–231.
Salvati, L., Ferrara, A., 2015. Validation of MEDALUS Fire Risk Index using Forest Fires Statistics through a multivariate approach. Ecol. Indic. 48, 365–369.
Shen, X.J., An, R., Feng, L., Ye, N., Zhu, L.J., Li, M.H., 2018. Vegetation changes in the three-river headwaters region of the Tibetan Plateau of China. Ecol. Indic. 93, 804–812.
State Forestry Administration of China, 2015. The 5th public report of the desertification and sandy desertification in China.
Sterk, G., Boardman, J., Verdoodt, A., 2016. Desertification: history, causes and options for its control. Land Degrad. Dev. 27, 1783–1787.
Sun, B.F., Wang, X.K., 2015. On assessment of sandy desertification sensitivity in Xinjiang. J. Southwest China Normal Univ. 40 (7), 108–112 (in Chinese).
Symeonakis, E., Karathanasis, N., Koukoulas, S., Panagopoulos, G., 2016. Monitoring sensitivity to land degradation and desertification with the environmentally sensitive area index: the case of Lesvos Island. Land Degrad. Dev. 27, 1562–1573.
Tan, M.H., Li, X.B., 2015. Does the green great wall effectively decrease dust storm intensity in China? A study based on NOAA NDVI and weather station data. Land Use Policy 43, 42–47.
Tavares, J.D.P., Isaurinda, B.A., Ferreira, A.J.D., Amiotte-Suchet, P., Coelho, C., Gomes, S., Amoros, R., Dos Reis, E.A., Mendes, A.F., Costa, L., Bentub, J., Varela, L., 2015. Assessment and mapping the sensitive areas to desertification in an insular Sahelian mountain region Case study of the Ribeira Seca Watershed, Santiago Island, Cabo Verde. Catena 128, 214–223.
Tian, F., Fensholt, R., Verbesselt, J., Grogan, K., Horion, S., Wang, Y.J., 2015. Evaluating temporal consistency of long-term global NDVI datasets for trend analysis. Remote Sens. Environ. 163, 326–340.
United Nations Convention to Combat Desertification, 1994. United Nations convention to combat desertification in countries experiencing serious drought and/or desertification, particularly in Africa. A/AC, 241/27, Paris.
United Nations Convention to Combat Desertification, 2012. Zero Net Land Degradation: A Sustainable Development Goal for Rio + 20. UNCCD Secretariat Policy Brief, 2012, 5.
Wang, T., 2004. Study on sandy desertification in China-3. Key regions for studying and combating sandy desertification. J. Desert Res. 24 (1), 1–9 (in Chinese).
Wang, X.M., Chen, H.F., Hasi, E., Li, J.C., 2008. Desertification in China: an assessment. Earth-Sci. Rev. 88, 188–206.
Wang, X.M., Hua, T., Lang, L.L., Ma, W.Y., 2017. Spatial differences of aeolian desertification responses to climate in arid Asia. Global Planet. Change 148, 22–28.
Wang, Y.H., Zhang, L.B., Guo, Y., He, P., Liu, W.L., Du, J.Q., Wang, L.X., 2014. Analysis of spatiotemporal pattern and tendency of land desertification sensitivity in six provinces of China. Res. Soil Water Conserv. 21 (5), 132–143 (in Chinese).
World Bank, 2009. In: Gender in Agriculture Sourcebook. World Bank Publications, pp. 454 ISBN 978-0-8213-7587-7.
Wu, S.H., Yin, Y.H., Zheng, D., Yang, Q.Y., 2005. Aridity/humidity status of land surface in China during the last three decades. Sci. China Ser. D 48, 1510–1518.
Xie, X.H., Liang, S.L., Yao, Y.J., Jia, K., Meng, S.S., Li, J., 2015. Detection and attribution of changes in hydrological cycle over the Three-North region of China: climate change versus afforestation effect. Agric. For. Meteorol. 203, 74–87.
Xin, Y.J., Du, T.Y., Xin, Y.C., Wu, A.D., Lu, F.G., 2011. The evaluation of carrying capacity of grassland in Qinghai. Qinghai Prataculture 20, 13–22 (in Chinese).
Xu, D.Y., Ding, X., 2018. Assessing the impact of desertification dynamics on regional ecosystem service value in North China from 1981 to 2010. Ecosyst. Serv. 30, 172–180.
Xu, D.Y., Li, C.L., Song, X., Ren, H.Y., 2014. The dynamics of desertification in the farming-pastoral region of North China over the past 10 years and their relationship to climate change and human activity. Catena 123, 11–22.
Yu, M., Wang, G.L., Parr, D., Ahmed, K.F., 2014. Future changes of the terrestrial ecosystem based on a dynamic vegetation model driven with RCP8.5 climate projections from 19 GCMs. Clim. Change 127, 257–271.
Zewdie, W., Csaplovics, E., Inostroza, L., 2017. Monitoring ecosystem dynamics in northwestern Ethiopia using NDVI and climate variables to assess long term trends in dryland vegetation variability. Appl. Geogr. 79, 167–178.
Zhang, G.L., Dong, J.W., Xiao, X.M., Hu, Z.M., Sheldon, S., 2012. Effectiveness of ecological restoration projects in Horqin Sandy Land, China based on SPOT-VGT NDVI data. Ecol. Eng. 38, 20–29.
Zhang, Z.H., Huisingh, D., 2018. Combating desertification in China: monitoring, control, management and revegetation. J. Clean. Prod. 182, 765–775.
Zhou, W., Gang, C.C., Zhou, F.C., Li, J.L., Dong, X.G., Zhao, C.Z., 2015. Quantitative assessment of the individual contribution of climate and human factors to desertification in northwest China using net primary productivity as an indicator. Ecol. Indic. 48, 560–569.